Update on SUSAN Concept Vehicle Power and Propulsion System

Jeffryes W. Chapman,[1] Jonathan L. Kratz,[2] Timothy P. Dever,[3] Arman Mirhashemi,[4] Erik J. Stalcup,[5] William R. Sixel,[6] Andrew A. Woodworth,[7] Ralph H. Jansen[8]
NASA Glenn Research Center, Cleveland, Ohio 44135, U.S.A.

Nic Heersema[9]
NASA Armstrong Flight Research Center, Edwards, CA 93523, U.S.A.

This paper provides an update on the power and propulsion (P&P) system design for the SUbsonic Single Aft eNgine (SUSAN) Electrofan. The SUSAN vehicle concept is a transformative concept hybrid electric aircraft with a single tail-mounted turbofan engine that provides thrust and power to 16 electric propulsors located on the wings. This configuration makes uses of large-scale power extraction along with a high-power electrical system transmitting 20 MW of power from the engine to the wing propulsors. This paper goes into detail on P&P advances relating turbine engine design, electrical system capabilities, advanced turbine control techniques, and electrical system cooling techniques. It should be noted that the SUSAN concept continues to be developed and this paper simply offers an update on the design.

I.   Introduction

The SUbsonic Single Aft eNgine (SUSAN) Electrofan is a new NASA regional transport aircraft concept. The SUSAN is a 180 passenger regional aircraft concept designed with the intent of reducing emissions by 50% while retaining the speed, size, and range typical of large regional jets [1]. The SUSAN aircraft concept is one that seeks to combine various technologies, each with their own small benefit, to produce a substantial benefit at the system level. This paper documents an update on SUSAN power and propulsion (P&P) system relative to the study detailed in Ref. [2].

A schematic of the relevant subsystems is included in Figure 1. Here it is shown that SUSAN is powered by a single turbofan engine that powers 16 individual wing mounted propulsors. Power is transmitted to these propulsors using four 5 MW generators connected to the engine shafts. Wing propulsors are each driven by two counter rotating electric motors with grid stabilization and augmentation provided by a rechargeable battery. Additionally, non-rechargeable batteries are used to provide power to the wing propulsors in the case of a potential engine failure scenario. This single engine configuration results in a simplified overall architecture, which reduces complexity, weight, and cost.
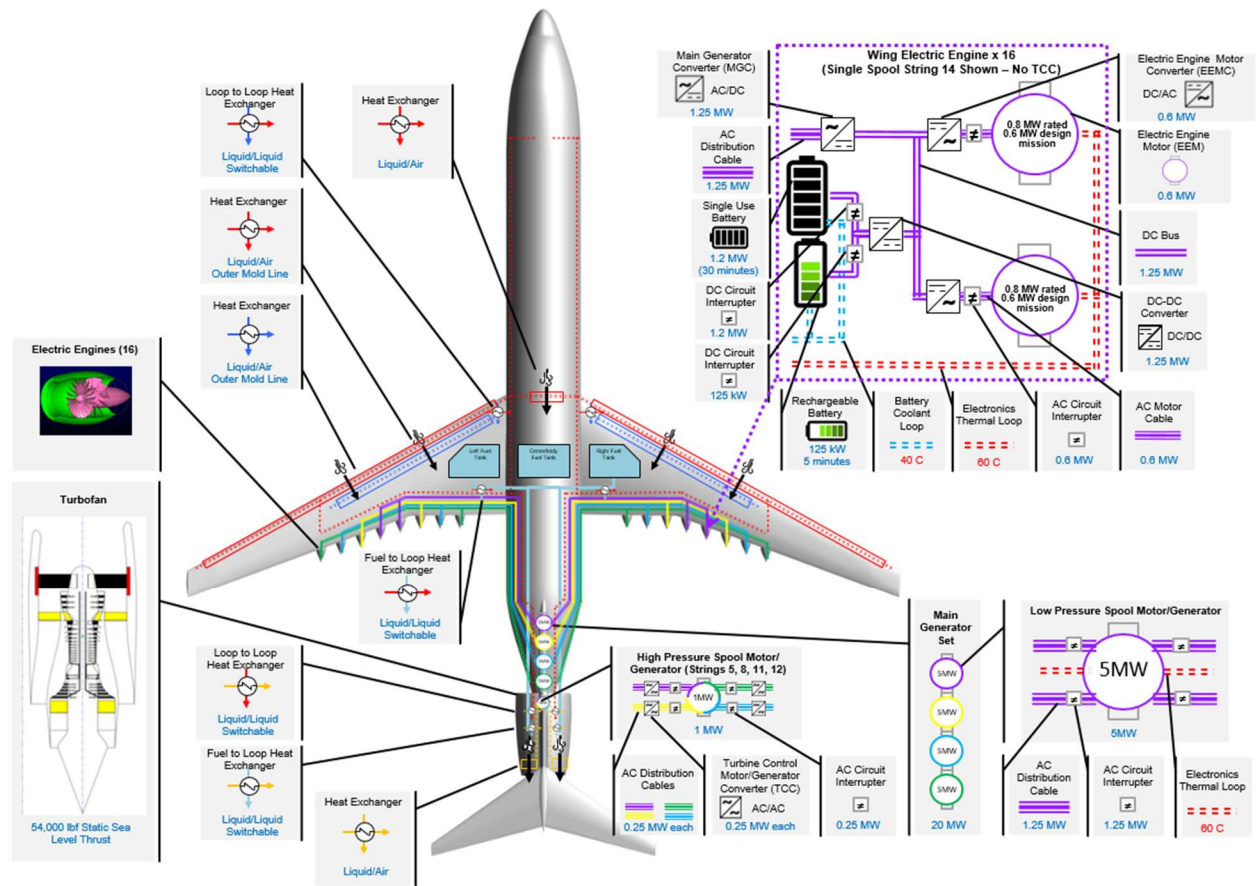

Figure 1. SUSAN turbofan engine.

The advanced turbine engine for the SUSAN makes use of several novel and advanced technologies that come together to provide benefits in thrust specific fuel consumption. These technologies include low pressure ratio fan and wing fans (1.37 and 1.25 respectively), boundary layer ingestion, fan gearbox, large scale power extraction, high pressure ratio core, high temperature combustor inlet, variable area bypass and wing propulsor nozzles, and an optimized split of thrust generated between the tail mounted engine and the wing propulsors. Additionally, the SUSAN engine makes use of the novel turbine electric energy management (TEEM) concept, where power is applied or removed from the engine shafts to dampen out transient behavior. Considering these technologies, the overall P&P system offers a 22% reduction in thrust specific fuel consumption relative to the state of the art.

The electrical system considers advanced power electronics, motors, batteries, transport system, and thermal management system. Updates on the electrical power system (EPS) cover electric machines, converters, cables, and the DC bus. First, the electric machines to be implemented are discussed, the wing engine machine, and the main generator. Next, updates on the requirements, topology, and approach for the EPS converters are discussed. The approach to electrical cable selection and modelling is then covered; and finally, reasons for, and the implications of, the change in the DC bus approach from an unregulated to a regulated configuration are discussed. An update on the thermal management system includes the rationale for the system architecture, the evaluation and selection of coolants, and further studies on potential heat rejection mechanisms.

Topics discussed in this paper are the turbofan engine (and the propulsion system thrust ratio) in Section II, the electrical power system components (engines and generators) in Section III, the advanced engine controls (TEEM) in Section IV, the thermal system in Section V, and conclusions in VI.

II.   Turbofan Engine and Propulsion System Thrust Ratio

This section covers the turbofan engine and the Propulsion System Thrust Ratio, that is, the ratio of engine thrust to the thrust produced by the electric motor wing propulsors.

A. SUSAN Turbofan Engine

The SUSAN P&P system uses a single geared turbofan to generate power for the wing propulsors and for generating thrust. A diagram of the engine architecture is in Figure 2. Engine architecture [3] considers a two-spool engine using a fan, 3 stage low-pressure compressor (LPC), and 4 stage low-pressure turbine (LPT) on the low-pressure spool (LPS) and a 13-stage high-pressure compressor (HPC) and 2-stage high-pressure turbine (HPT) on the high-pressure spool (HPS). Power extracted from the engine for the wing propulsors is taken predominately from the LPS with a small amount taken from the HPS at certain operating conditions for operability purposes.
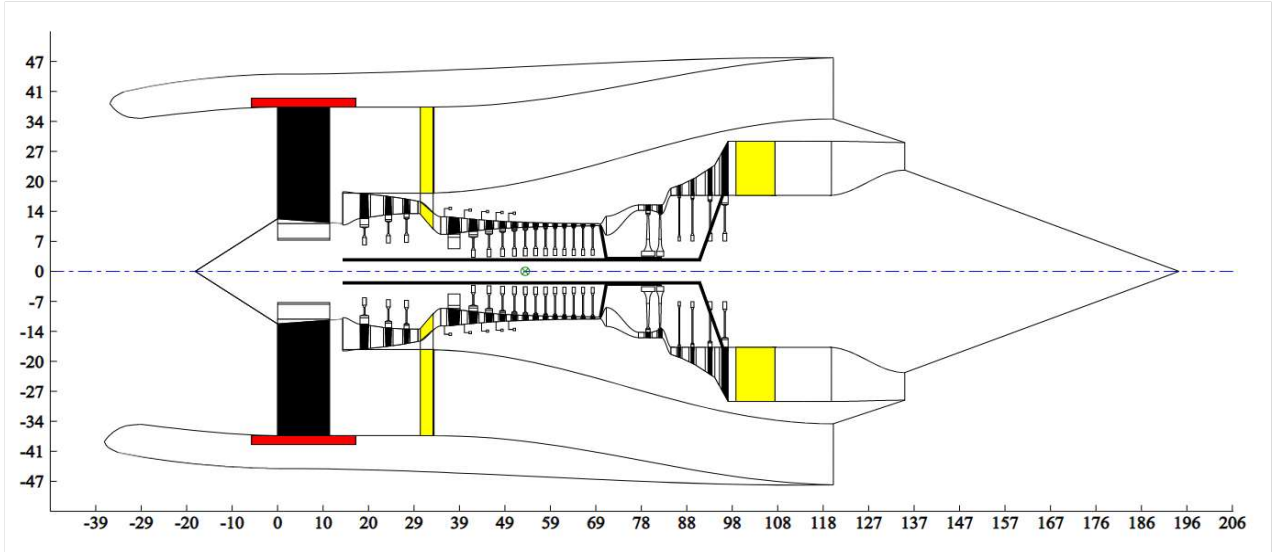

Figure 2. SUSAN turbofan engine.

Engine design was completed using a three-point MDP that considers top of climb (TOC), cruise (CRZ), and rolling take off (RTO) operating conditions. The engine is sized at the TOC point and uses the RTO maximum thrust demand as the main sizing limit. Power extracted for running the electric machines is completed mainly from the LPS with a small amount taken from the HPS at high power to accommodate engine operability, while also reducing the required size of the electric machines. [3] As a starting point, engine thrust requirements are estimated based on the Boeing 737 powered by two CFM LEAP-1B engines. These thrust requirements are then updated to include some margin and then reduced by 10%, as single fault scenarios in the SUSAN distributed propulsion system result in less thrust loss than a traditional two engine system. An overview of the design operating points is in Table 1. The thrust numbers signify total system thrust that includes the 16 wing fans. Considering only the fan air bypassing the core in the turbofan engine the bypass ratio is 5.66. However, if the wing propulsor flow is included as propulsion air that bypasses the core engine, the effective bypass (eBPR) is over 20. Adding the thrust of the wing propulsors to the thrust of the turbofan yields a TSFC of less than 0.43.

Table 1 : SUSAN engine thrust results from multi-design point.

Operating Point	Altitude (ft)	Mach number	total system net thrust (lbf)
Top of climb (TOC)	37000	0.785	11500
Cruise (CRZ)	37000	0.785	7134
Rolling takeoff (RTO)	0	0.25	46000

Compressor performance is set based on assumed pressure ratios for the fan (1.37), wing counter-rotating fan (1.25), and LPC (3.1). The HPC PR is limited by either the maximum HPC exit total temperature (Tt3max) or the minimum HPC exit corrected flow (Wc3min). For this study, the Tt3max was assumed to be 1810 ˚R (1350 ˚F) and the Wc3min was assumed to be 2.5 lbs/sec. With a single turbofan engine, the SUSAN turbofan the core airflow is much larger

than for an individual CFM LEAP-1B engine. The result is that while the LEAP-1B reaches the Wc3min before the Tt3max, the HPC PR in the SUSAN turbofan continues to increase until the Tt3 limit is reached at a HPC PR of 20.25. The result is that the overall pressure ratio (OPR) of the LEAP-1B is roughly 40, while the SUSAN turbofan has an OPR of 86. In the Brayton cycle the thermal efficiency of the core engine is a direct function of OPR. Thus, the higher OPR of the SUSAN yields a higher thermal efficiency in comparison to the LEAP-1B.

Turbomachinery efficiencies are assumed to be advanced, with wing fan efficiency at 96%, and engine fan, LPC, HPC, HPT, and LPT efficiencies between 90% and 92%. It has been determined that 35% of the thrust should come from the engine at cruise and at the other operating points the thrust split is set based on engine operability requirement and weight concerns, as detailed below.

Boundary layer ingestion (BLI) is considered for the turbofan engine by estimating radial pressure drops associated with the BLI using computational fluid dynamics (CFD). This information is then passed into the engine model using a mass flow averaged pressure. Accounting for changes in momentum and pressure drag the engine thrust is recalculated to determine the BLI benefit.

B. Propulsion System Thrust Ratio

Propulsion thrust ratio is a major contributor to the SUSAN overall design. For this paper, thrust ratio is defined as the ratio of thrust produced by the main engine and the total propulsion system thrust, which includes the engine thrust and the thrust produced by the wing propulsors (Engine Thrust / Total Propulsion System Thrust). Therefore, a 0% thrust split would show a configuration that is driven only by the electrical propulsors. This split is used to size the engine fan, wing propulsor fans, and electrical system. Updates in the thrust ratio also creates changes in aircraft design choices such as tail design, and wing propulsor structural needs. Three studies were conducted to determine the thrust ratio: a TSFC comparison, a weight comparison, and a reliability study.

The TSFC comparison is completed by resizing the engine and components while specifying different thrust ratios. There are two considered cases, propulsion system with no boundary layer ingestion (BLI) effects and a model that considers BLI on the engine only. Wing propulsor BLI effects are not considered in either analysis because the final placement of the propulsors on the wings was not settled at the time of this study. Results of the study can be seen in Figure 3. Here it can be seen that TSFC increases with an increase in thrust ratio. This is mainly due to the very low-pressure ratio of the wing propulsors and high electrical system efficiency. However, considering BLI for the engine results in an opposite trend, where TSFC is reduced with increasing thrust ratio with lower TSFC as thrust ratio increases because more BLI air is moving through the bypass and less through the core If the wing propulsor BLI was also included, it would increase the efficiency of producing thrust with the wing propulsors causing the TSFC of low thrust ratio concepts to reduce and potentially making the low thrust ratio concepts more efficient than high thrust ratio concepts. This study offers a progression in the thrust ratio selection, but more work is needed to completely understand the tradeoffs for maximizing TSFC.
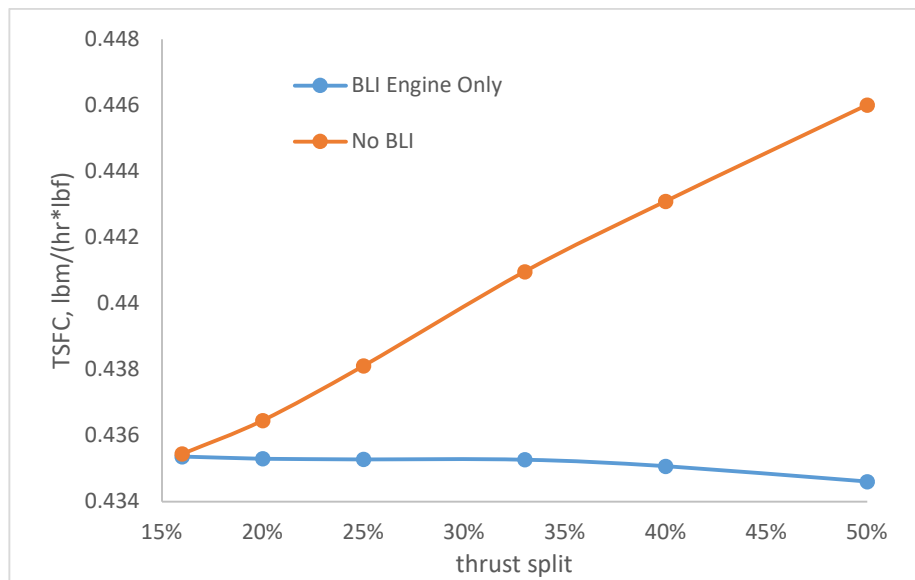

Figure 3. Thrust ratio vs. TSFC.

Weight estimation is developed by combining the engine and wing propulsor weights, developed by extrapolating values estimated in the WATE++ software, and with the electrical system weight, developed using specific power numbers provided for SUSAN electrical system weight estimation by Haglage [4]. For this study three total system weight-to-power were calculated by adding up the weight-to-power of each electrical component in the electrical system architecture, maximum, minimum, and nominal. AC cables for the designs are assumed to be 20 m in length and DC cables are assumed to be 1 m in length These calculations result in a nominal weight-to-power of 0.093 kg/kW for minimum, 0.21 kg/kW for nominal, and 0.63 kg/kW for maximum. Stack plots of each configuration are shown in Figure 4. In the nominal and maximum electrical weight-to-power traces minimum overall weight can be achieved by increasing the thrust ratio. In the minimum electrical weight-to-power this trend flips, and minimum overall weight is achieved with a low thrust ratio.
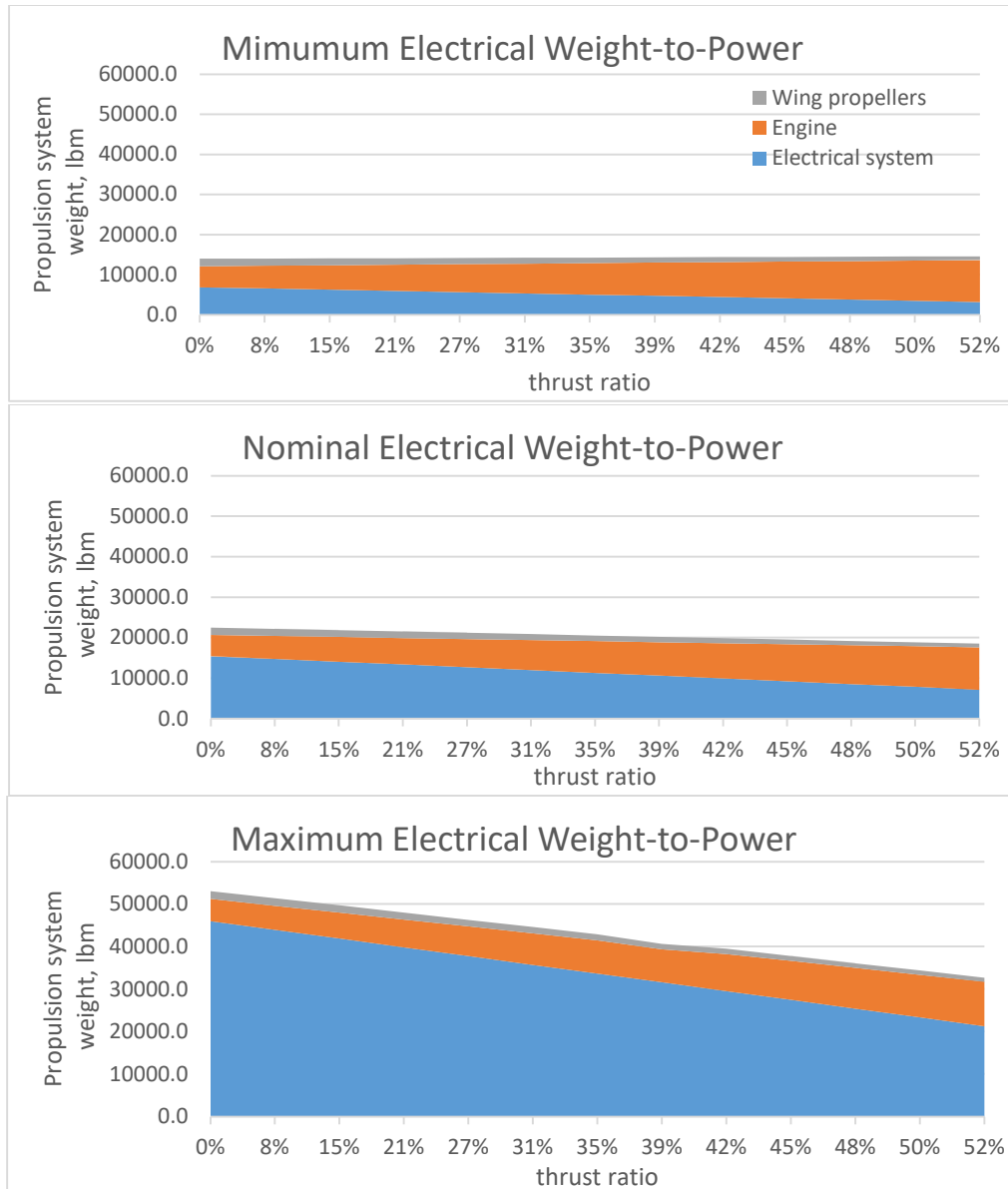

Figure 4. Propulsion system weight stack graphs for maximum, nominal, and minimum electrical system weights.

Overview of weight values at 0% and 50% thrust ratios is shown in Table 2. Engine weight reduction observed with decreasing thrust ratio is due mostly to decreases in fan, nozzle, and nacelle size. Wing propellers increase in weight by roughly 2x as the thrust ratio is decreased. Similar trends can also be observed in the electrical weights, where weight is increased by 2x as thrust ratio decreases. Differences in weight between the maximum, nominal, and minimum reflect the differences in weight-to-power. The final values for total values can also be seen. They show that the differences between 0% and 50% for nominal and maximum total weights are 3700 lbm and 18740 lbm, respectively. This difference for the minimum total weight is 550 lbm. This shows, that in all but the most optimistic scenario lower thrust ratio configurations will weigh more.

Table 2 : Engine power requirements and velocities for the main mission point types.

Subsystem weight	thrust ratio 0%	thrust ratio 50%	weight units
Engine	5231	10037	lbm
Wing propellers	1872	992	lbm
Min. electrical	6850	3475	lbm
nominal electrical	15413	7818	lbm
Max. electrical	45996	23331	lbm
Min. total	13953	14504	lbm
nominal total	22516	18847	lbm
Max. total	53098	34360	lbm

A reliability study was also conducted. In this study, a maximum required aircraft thrust is determined for single fault scenarios. This is typically reflected in the engine requirements and for SUSAN, thrust requirements are estimated to be two of baseline engines (CFM LEAP-1B). However, with SUSAN, the single fault scenario changes the equation. To estimate the thrust requirements, two baseline engines are assumed to produce 100% total thrust. During normal operation, only 90% of this total thrust is used in an RTO scenario. This overdesign is done so that 50% thrust can be used for RTO in a single-fault scenario (single engine out). However, this is not the case for the electrically driven propellers. On SUSAN, there are 16 such propellers driven. Previous work has shown various configurations in which a single fault could eliminate 1, 4, or 8 of these propulsors [4]. Single fault thrust for each of the fault scenarios is shown in Figure 5 as a function of thrust ratio. Here 90% thrust represents the maximum thrust required for the propulsion system under typical operation and 50% thrust is required for any single-fault situation (red line). Each system is designed to meet the 90% thrust in an absence of a fault. For the 1 and 4 fault scenarios the thrust can be provided regardless of the thrust ratio. In the 8 fault scenarios the 50% thrust limit cannot be met under 7% thrust ratio. Similarly, in the engine fault scenario the 50% thrust limit cannot be met over 40% thrust ratio. Therefore, the total system thrust requirement can be updated from 100% to 90% for all system architectures if the system is designed between 7% and 40% thrust ratio.
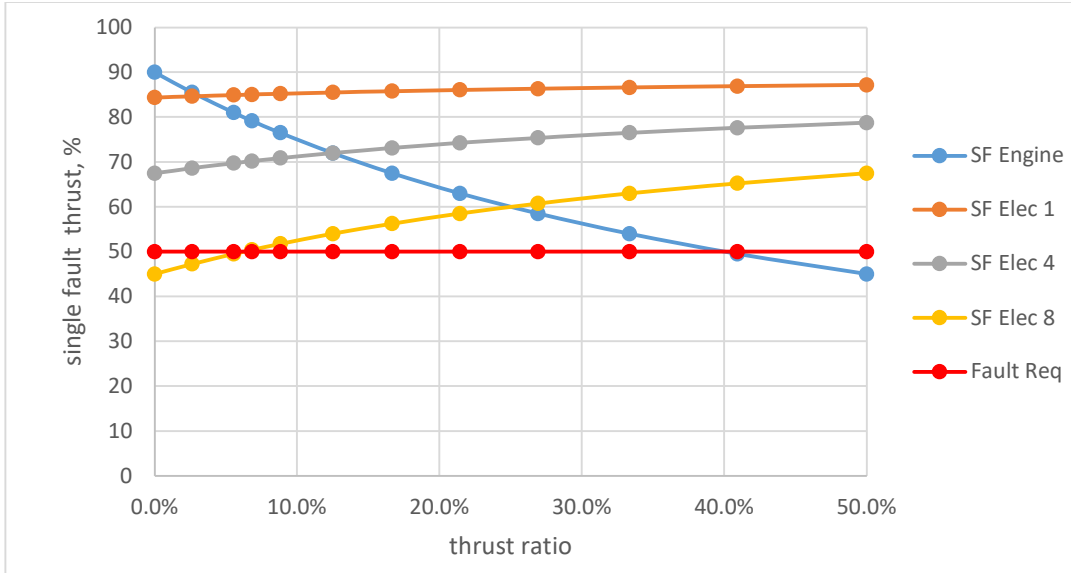
Figure 5. Single fault (SF) thrust with different failure scenarios.

Considering each of the studies it was determined to move forward with a thrust ratio of 35%. This was selected because weight would most likely increase with decreasing thrust ratio and the thrust ratio must stay under 40% (Note, 35% was selected to provide some margin). The TSFC was not used as a metric, due to uncertainty surrounding the effects of BLI on the wing propulsors.

III.   Electrical Power System Components

This section covers the SUSAN electrical power system (EPS components. Topics covered are the electric machines, the inverters, the cables, and updates to the DC bus configuration.

A. Electric Machines

There are two electric machines covered here; the wing engines, and the generator. The wing engine are based on the HEMM (High Efficiency Megawatt Motor), a megawatt class wound field synchronous motor with a stretch performance goal of 16 kW/kg and efficiency of 99 percent. HEMM is a partially superconducting, synchronous wound field machine that can operate as a motor or generator, as shown in Figure 6 [5]. HEMM combines a self-cooled, superconducting rotor with a semi-slotless stator, allowing the motor to achieve high specific power and efficiency without requiring the external cooling commonly needed in superconducting machines [6].   The combination of the described elements allows a motor to be built that essentially operates like any traditional, i.e. non-superconducting), motor when viewed externally as a system, however it incorporates superconductors on the rotor to create a strong airgap magnetic field that enables specific power and efficiency performance that cannot be achieved using normal conductors or permanent magnets.   The SUSAN generator is a 5 MW machine, based on the HEMM technology.
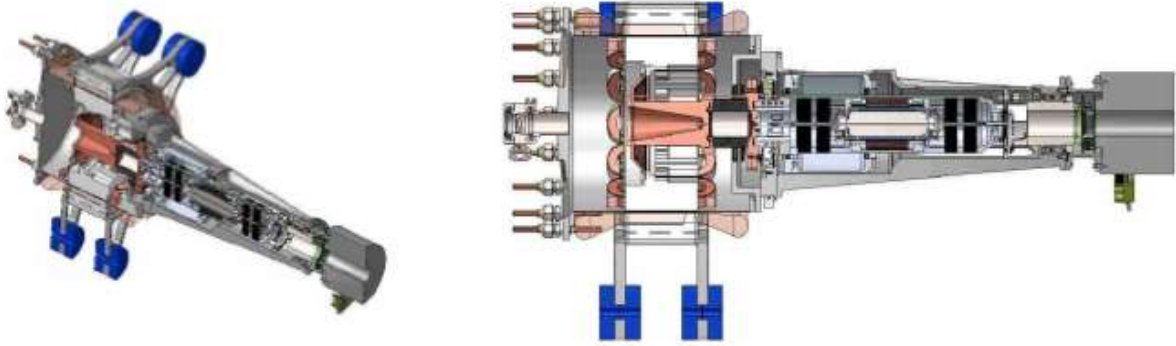
Figure 6. High Efficiency Megawatt Motor (HEMM) design.

B. EPS Converters

The converters for the EPS are based on the HEATheR design. The design goal of the converter is to enable the achievement of three key performance parameters: high efficiency (99.5%), high power density (20 kW/kg), and low harmonic distortion to limit HEMM rotor loss. These three parameters are typically in conflict with one another when trading converter designs, and therefore topology decisions must carefully achieve balance between them [7].

The multilevel switching architecture is implemented to lower the current waveform distortion and enable use of high efficiency and readily available off-the-shelf Silicon Carbide MOSFETs in a higher voltage system. The very low switching losses and low conduction losses of the Silicon Carbide MOSFETs enables the high efficiency target.

Interleaving filters are implemented to enable equal current sharing among parallel FETs, providing significant current waveform distortion reduction. These filters are designed with high inductance to minimize circulating current in the converter and the associated losses. Custom filters consisting of soft magnetic material developed and engineered by the NASA Glenn advanced magnetic materials group is used to minimize the mass and loss impact of these filters.

Another vital aspect of the converter's design is its controller. HEMM is very susceptible to spatial harmonics due to the machine's low inductance; small perturbations in the back-emf can lead to large current harmonics. In particular the 3rd, 5th, and 7th harmonics need to be suppressed to avoid the associated rotor loss. A harmonic controller is incorporated to accomplish this harmonic suppression, which augments the classic vector control.

Additionally, for this type of machine, minimizing cryogenic heat load is critical for high machine performance. Rotor eddy current loss is a difficult heat load to manage, due to current ripple from the motor drive. The motor drive concept design described above is used to achieve high performance metrics with little current ripple – the goal of the final design being to generate less than 5 W of magnetic loss in the rotor. [8].

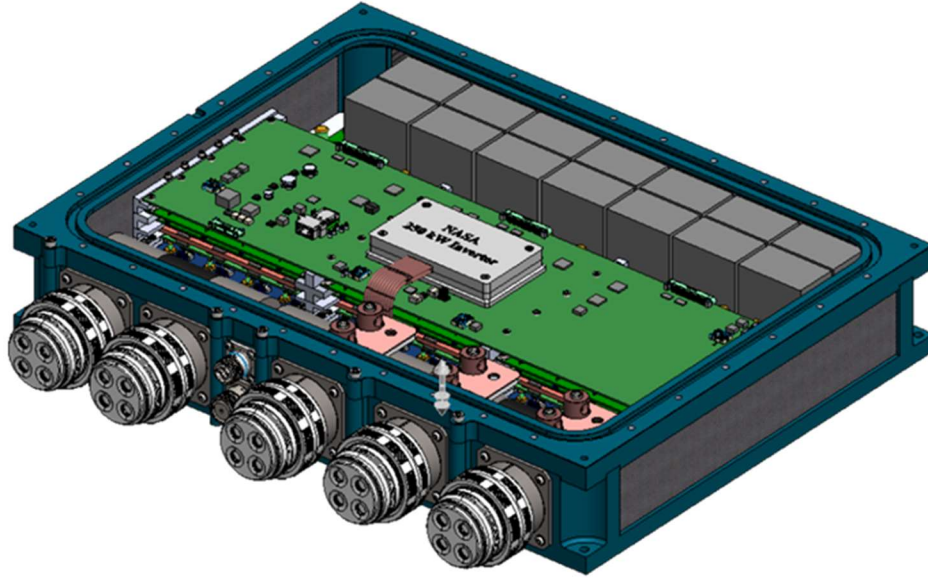A rendering of a low power prototype HEMM Converter is shown in Figure 7.

Figure 7. Low Power Prototype HEMM Converter Design

C. **Electrical Cables**

Using ampacity adjustments for the appropriate thermal environment, a model was developed for electrical cable mass and loss key performance parameters (KPPs) for megawatt (MW) electrified aircraft propulsion (EAP) [9]. The identified cable KPPs are related to weight and loses, as expected; they are the specific weight $W_{s.l.,s.p.}$, [kg/m/MW], and cable power loss at I_{rated} per length, $P_{CR\,s.l.}$ [W/m]. This model will be used in cable sizing for, and modeling of, the SUSAN aircraft.

D. **DC Bus Configuration Updates**

The original Electrical System Trade Study for SUSAN Electrofan Concept featured a DC Bus unregulated [2]. The advantage of this approach was that the mass of the DC-DC converter was saved. In this configuration, the battery voltage was allowed to droop; thus, the DC bus voltage would be allowed to change throughout the mission based on the battery state of charge (SOC); and any difference between the Main Generator Converter (MGC) output voltage and the battery voltage would result in a battery charge or discharge. Unfortunately, this approach would require that the EPS system be able to operate at a higher DC current, which would increase the weight of EPS equipment (cable, converters, machines, contactors) due to I^2R resistive losses. Also, in this configuration, maintenance of the battery charge/discharge rates would be extremely difficult, and the control would be more complex, especially in failure modes. For this reason, the switch was made to a regulated DC bus.

In the updated configuration, a DC-DC converter is added between the batteries and the DC bus (see comparison, Figure 8). The battery voltage will still be allowed to vary over the mission, but DC the bus voltage will not. Although this approach will incur the additional mass of a DC-DC converter, advantages are that the EPS equipment can be lower mass (sized for higher voltage, lower current), and maintenance of the battery charge/discharge rates becomes straightforward: the battery SOC control will be defined by a combination of Supervisory Control and bus current requirements. A further advantage is that the overall control is more straightforward, especially in failure modes.
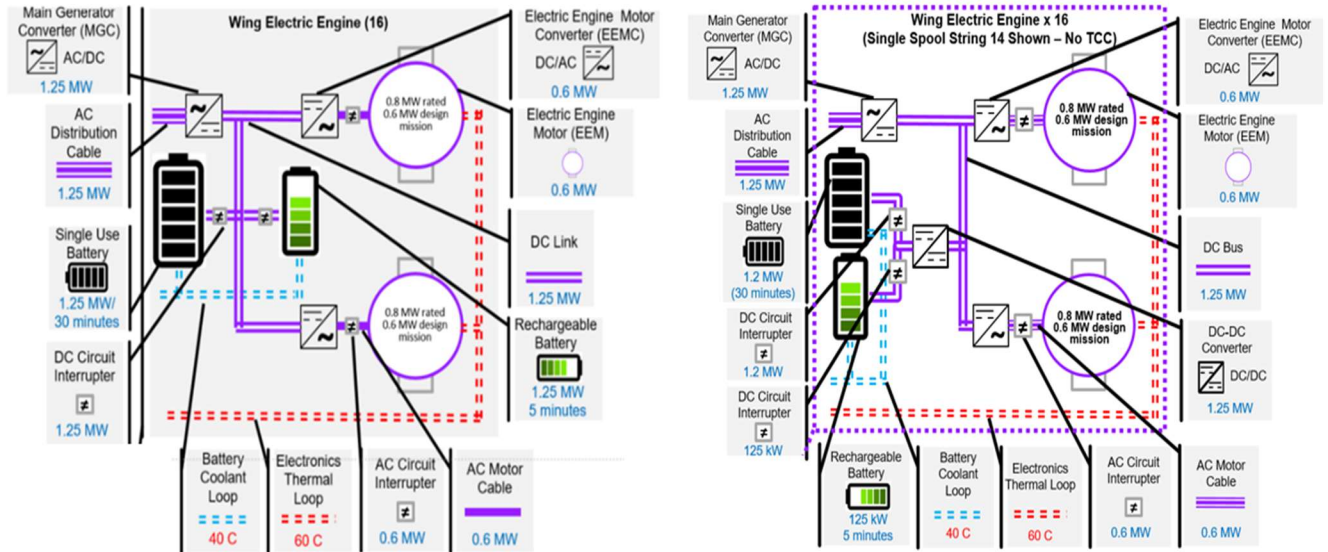
Figure 8. Original (left) and updated (right) DC Bus

IV. TEEM Control

SUSAN combines various technologies to aggregate an overall benefit. TEEM is one of the technologies it utilizes. TEEM is a controls approach that utilizes an electric power system integrated with turbomachinery to improve the operation of the engine to the benefit of the overall system [10]. Several applications have been covered in the literature [11,12,13]. Primarily the focus has been on improving transient operability with the goal of alleviating design constraints on the engine such that performance improvements related to efficiency and weight can be achieved. The approach is to apply torques to the engine shafts with electric machines such that the engine, and the compressors, exhibit quasi-steady-state operating conditions through a change in rotational speed and power. This paper will approximate the requirements for the electrical power system needed to implement TEEM and use those results to infer the impact that can be made with the electrical power system that is already inherent with the SUSAN concept.

To implement TEEM, an electrical power system must be present. This entails using electric machines coupled to the engine shafts and an energy storage system. Torque in addition to the torque imparted on the engine shaft through the gas path as controlled by the fuel flow rate, can be applied to modify the operation of the engine. Engine transients are the focus of this application and refer to changes in the operating condition of the engine that are primarily associated with rapid changes in thrust/power demand. Thrust is often corelated with engine fan speed for control. To achieve the desired thrust or power level, the engine shaft speeds must change and the means of doing this is to change the fuel flow rate. Due to the significant inertia of the engine shafts, the shaft speed response lags the fuel flow input. A mismatch in internal air flow and shaft speed results. This can lead to off-incidence flow impinging on the compressor blades that pushes one of the compressors in the engine closer toward a stall or surge condition. This effect can be viewed on a compressor map such as those shown in Figure 9. The maps define the performance of the compressors within their operability range, which has an upper bound set by the stall/surge line. The map relates the metrics of pressure ratio, adiabatic efficiency, corrected mass flow rate, and corrected speed (shown in Figure 7 by the curved line extending down from the stall/surge line). The steady-state operating line (shown in red in Figure 7) defines the steady-state performance of the engine across its power range for a given operating condition (altitude, Mach number, etc.). During transients, the operating point on the compressor maps will deviate from the steady-state operating line and define a running line. Typically, the HPC running line will move closer to the stall line during an acceleration. The same is true for the LPC running line during decelerations. This is illustrated in Figure 9.
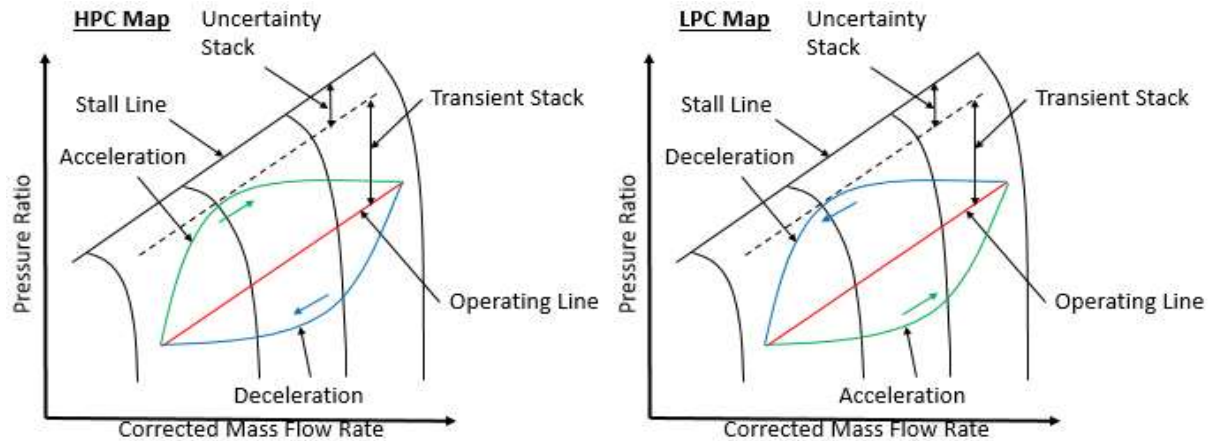
Figure 9. Illustration of HPC and LPC maps with stall margin impact noted for an acceleration and deceleration. [10]

By applying torques to the shafts with electric machines to add or extract power that is supplied or absorbed by an energy storage system, the deviation from the steady state operating line can be reduced. Tighter regulation of transient operability can alleviate constraints on the engine design and lead to more efficient and lighter weight engines. Ref. [14] and [15] describe some of the operability issues created by engine transients and allude to the impact they have on engine design, often resulting in composes the reduce efficiency. A dynamic model of the SUSAN propulsion system, as of the time of this paper, was created. A controller was developed for nominal operation. This included the development of various setpoint schedules, actuator schedules for the variable bleed valve (LPC stability bleed), and variable area fan nozzles for both the engine and wing fans. A Proportional Integral (PI) controller with limit logic is used to command the fuel flow rate necessary to meet the desired engine corrected fan speed. The engine and wing fans are coordinated through the transfer of various pieces of information. The engine supplies corrected fan speed to the wing fan controller which uses that information along with the flight conditions to determine the wing fan corrected fan speed setpoint. A PI controller closes the loop on the corrected fan speed using the wing fan motors. The wing fan power demands are supplied to the engine controller to calculate a base power extraction demand and a PI controller for managing the state of charge of the energy storage device(s) is implemented to command any additional power extraction/injection relative to this value such that power is consumed as desired.

A TEEM controller was developed and integrated with the controller described above. The TEEM strategy employed her is mostly consistent with the strategy defined in [11] and [13]. The approach included of utilizing a PI controller to coordinate the HPS shaft speed with the commanded fuel flow rate and flight conditions during accelerations. This tends to result in power injection. When TEEM is being discussed a power injection or extraction will be made in reference to the nominal power extraction that is commanded from the shaft to meet the demand of the wing fans and other aircraft systems. Unlike some prior applications of TEEM in literature, the LPS electric machine was also utilized during accelerations and PI controller coordinated the LPC PR with the commanded fuel flow rate and flight condition. The purpose for using the LPS EM during accelerations was to alleviate an issue observed with HPS speed overshoot, which is believed to be related to significant differences in shaft inertias between the spools that is further exacerbated by large power extraction loads that are disproportional and growing throughout the acceleration transient. During decelerations, the LPC PR controller commands a power extraction from the LPS, and that power is transfer to the HPS to further enhance the operability impact while dissipating excess power. The TEEM controller includes activation/deactivation logic like Ref. [10]. In addition, logic was added to prevent TEEM from sourcing power from the energy storage device(s) once a minimum state of charge was reached.

The power system inherent with SUSAN is very capable for implementing TEEM without much additional modifications. Electric machines integrated with the engine are sized for power extraction. The only feature that TEEM might have implications on is the size of the reusable energy storage system. A subjective decision informed through some analysis and engineering judgement was made to set the energy storage size at 12.5kW-hr. This amount of energy storage on demand enabled power injections of up to 1750 hp and 1500 hp during accelerations on the HPS and LPS respectively. The power system power and energy capabilities could be increased to improve the operability impact, thus opening up more opportunities for operability influenced design benefits, Alternatively, the power system capabilities could be reduced to decrease energy storage requirement at the expense of some of the operability benefits.

To illustrate the operability improvement achieved with TEEM rapid acceleration and deceleration transients were simulated at sea level static (SLS) conditions (altitude = 0ft, Mach number = 0) and cruise (CRZ) conditions (altitude = 37,000ft, Mach number = 0.785). Figure 10 shows the HPC stall margin during the acceleration and LPC stall margin during the deceleration. Figure 11 shows the running line relative to the stall line. In the plot, PR refers to the pressure ratio and W_c is the corrected flow rate. The use of TEEM improved the minimum stall margin in all case and demonstrates an appreciable benefit on the compressor maps as indicated by suppression of the running lines away from the stall/surge line. One additional notable result is the reduction in HPS overspeed during the acceleration, that is indicated in the results without TEEM by the significant extension of the running line past the final operating point.
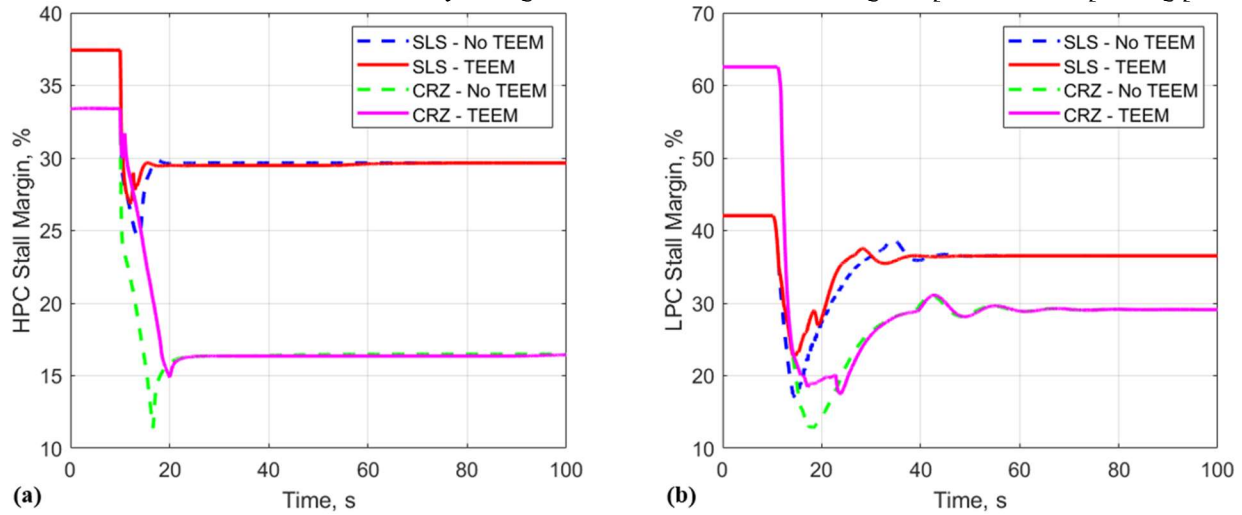

Figure 10. Stall margins during transient responses at SLS and CRZ conditions, both with and without TEEM. (a) shows the HPC stall margin during and acceleration and (b) shows the LPS stall margin during a deceleration.
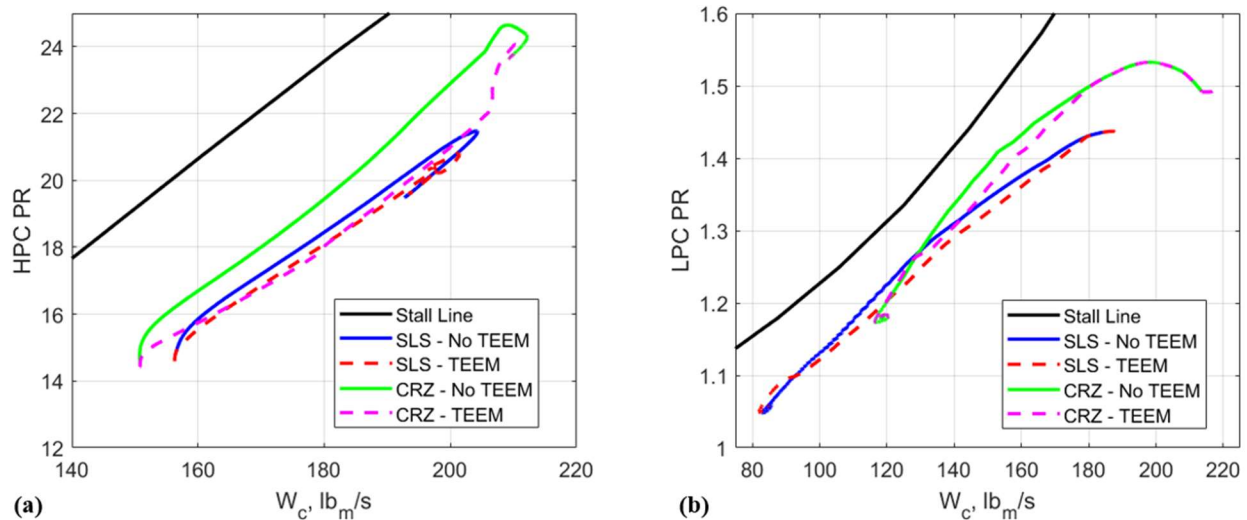
Figure 11. Transient running lines for transients at SLS and CRZ conditions, both with and without TEEM. (a) shows accelerations on the HPC map while (b) shows decelerations on the LPC map.

SUSAN remains a moving target seeking to achieve a more optimal design. The options for future work are rich and may include the introduction of boost during climb, which will require changes to the controller. The implementation of TEEM could be improved. A schedule-based approach that leveraged optimization techniques in its design has been developed in Ref. [16] and could be applied to SUSAN in a future design iteration. Finally, the

choice in energy storage size could be re-evaluated. If boost is applied and turns out to be advantageous, it could open make TEEM a non-factor in sizing of the reusable energy storage system and enable increases in power sourcing capabilities that will enhance the impact of TEEM.

V.   Thermal

High power, high efficiency components are required for the SUSAN propulsion and power system architecture. Even with high efficiencies, the heat generated by these components is significant, and must be managed appropriately in a variety of environments. Previous work explored different types of thermal management systems (TMS) and their ability to manage the entire heat load of the propulsion and power systems except the turbofan engine itself (which at this stage is assumed to have a TMS independent of the rest of the aircraft) [17].

A. Thermal Management System Architecture

The current TMS architecture is shown at a high-level in Figure 1. Detailed layout is in work and will focus on flow optimization and fault tolerance. The design uses two different thermal management loops that operate at temperatures appropriate for their thermal loads. These two loops service the batteries and electrical power system components. The trade study was begun with the initial assumption that three loops, which are optimized to the temperature of different load categories, would be a good architecture; however, as studies are conducted, it may be determined that a different number of loops is preferred. The loops utilize single-phase forced-convection liquid cooling as this is necessary to handle the high heat fluxes produced by the electronics. Forced-convection liquid cooling can attain higher heat transfer coefficients compared to air cooling and natural convection [18, 19]. Single -phase cooling is relatively simpler than two-phase and reduces sensitivity to body forces experienced in flight. Future trade studies will investigate higher heat flux thermal management technologies like two-phase systems, vapor-compression refrigeration, and thermoacoustic refrigeration [20, 21].

The first thermal management loop will service the battery system and operates nominally at 40 °C. Many battery chemistries exhibit reduced performance and degradation at temperatures below 20 °C and above 60 °C. The battery thermal management loop is planned to incorporate outer mold line cooling. Future work and trade studies are discussed a later section.

The second thermal management loop will service the electrical systems and operates nominally at 60 °C. The primary loads on the electrical systems loop are the electrical machines (motors and generators), which have a hot spot temperature limit around 200 °C, and the converters, which also have a limit of around 200 °C. The heat flux levels needed for both motor and converter are relatively high, requiring the cooling loop to have a significant temperature difference compared to the thermal limits of the electrical components. The electrical thermal management loop will be connected to an outer mold line surface heat exchanger as well as a liquid / air heat exchanger.

B. Coolant Selection

The range of acceptable temperatures for battery operation overlaps with that of liquid water, and battery thermal management systems likely would not benefit from direct cooling, e.g. immersion. Therefore, a non-dielectric fluid with greater thermal performance is a suitable choice. A propylene glycol/water mixture was selected due to its widespread usage and lower toxicity than ethylene glycol.

For the electrical power systems, direct cooling techniques are likely to be used for most if not all the components. Therefore, a suitable single-phase dielectric coolant must be selected. A commercial off the shelf coolant survey was completed for a variety of fluid compositions: aliphatic hydrocarbons (including alkanes, alkenes, petroleum-based oils, and PAO), aromatic hydrocarbons, silicate esters, silicones, fluorocarbons, hydrofluoroethers, and fluoroketones. Similar to past studies [22, 23, 24], a figure of merit (FOM) was developed to compare heat transfer performance (from local heat transfer coefficient) for a given pumping power. The FOM is based on the Mouromtseff number [25], which compares the relative heat transfer performance of different fluids for a given velocity. The FOM extends the Mouromtseff number by including some correction for the pumping power scaling of velocity and is specifically derived for fully developed turbulent flow (a = 0.8, b = 0.4, c = -0.25).

$$FOM = \rho^{a-c-1} \cdot c_p^b \, \mu^{b+c-a} \cdot k^{1-b} = \frac{\rho^{0.05} \cdot c_p^{0.4} \cdot k^{0.6}}{\mu^{0.65}}$$

The FOM at 60 °C is plotted in Figure 9 versus the flash point (or boiling point for fluorine-containing fluids). All fluids shown in Figure 12 have boiling points above 60 °C and most have a dielectric strength greater than 35 kV using ASTM D877. The flash point is an important parameter as the coolant may be in contact with or present near electrical components that are operating at high temperatures. While no single fluid type appears to have a clear advantage, PAOs generally have larger FOMs at flash points greater than 100 °C. PAOs are also have a widespread usage in the aviation industry. Therefore, a MIL-PRF-87252E PAO was selected as the SUSAN electrical power systems coolant. Also shown in Figure 12 is an area of desired performance for future coolant developments as a dielectric fluid with good thermal characteristics and higher flashpoint would offer direct cooling safe operation higher temperature range. The desired FOM is greater than 500, which is around the state of the art for PAO, and the desired flash point is greater than 220 °C as that is the upper limit of operation for many electrical machine and power electronics components.
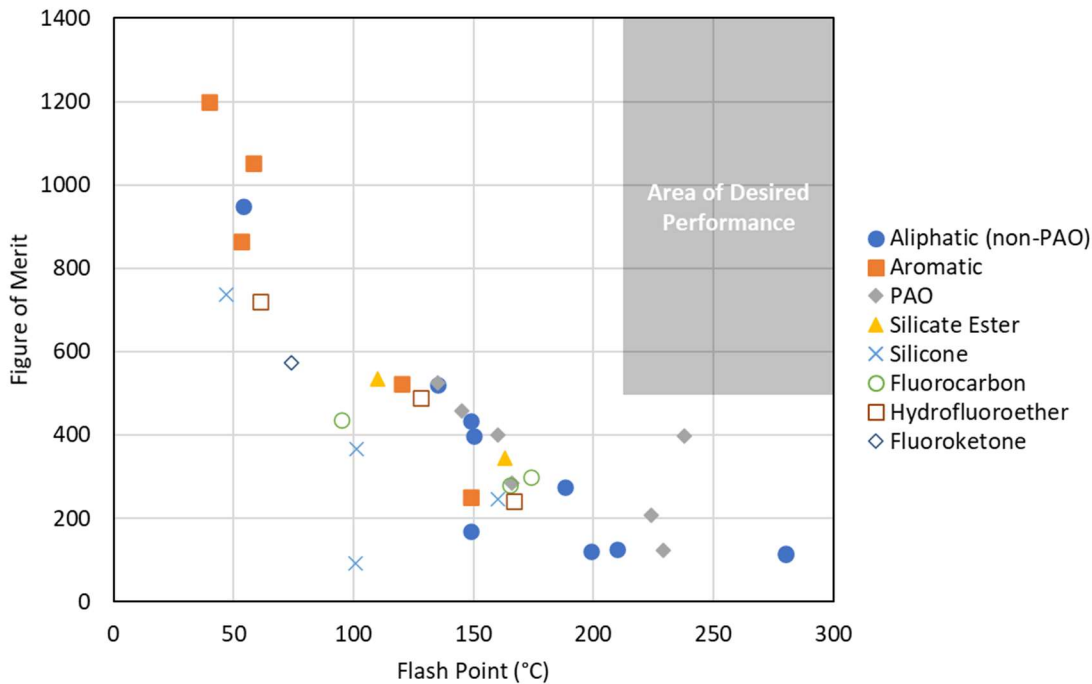

Figure 12. Figure of merit at 60 °C vs. flash point (or boiling point for fluorine-containing fluids) for various types of dielectric coolants.

C. Thermal Management System Evaluation

The previous work confirmed the expectation that no single type of TMS would be capable of managing the entire heat load, suggesting that the approach being pursued of using a combination of different methods of TMS where they will be most effective is the right approach to pursue [26]. Preliminary values for mass, power, and drag of traditional liquid / air heat exchangers (HEX) were calculated, along with mass and area for oscillating heat pipes (OHP), as shown in Table 3.

Table 3 : Summary of results [17].

		Oscillating Heat Pipes		Liquid / Air Heat Exchanger		
Loop	Heat Load (kW)	Mass (kg)	Area (m^2)	Mass (kg)	Power (W)	Drag (lbf)
Battery	222	147	24	80	81	13
Electronics	919	618	106	330	334	37

Given the different relevant parameters, these two methods cannot be directly compared except in terms of mass, an unfair comparison. To evaluate the methods against each other as part of an optimization effort, the change in block fuel burn is used an equivalencing parameter. The change in block fuel burn is determined by assessing the preliminary sensitivities of the block fuel burn for each mission type (design and economic) to changes in each of the design

parameters of interest individually. For the TMS, the parameters of interest are mass, power, and drag. As design of the overall SUSAN architecture is still underway, these sensitivities are changing. For the current analysis, preliminary sensitivities are calculated using the conceptual design described in Ref. [27] with the fully turbulent flow wing design described in Ref. [28] incorporated.

So far only the sensitivities for mass and drag have been determined; sensitivities due to power are complicated by the hybrid-electric architecture and haven't been assessed yet. Additionally, the parameters of interest were calculated only for the OHP and the liquid / air HEX independent of any support hardware and not including the system to extract the heat from the components and bring it to the heat rejection site. A more refined design is required before the relevant locations can be determined, and the mass and power of the transport system can be calculated. For this phase of the analysis, it is assumed that the mass and power required for transporting the heat would be the same for the OHP and the liquid / air HEX and may therefore be excluded from the comparison. With these limitations in mind, Table 4 provides a comparison between the OHP and liquid / air HEX in terms of increase to block fuel burn.

Table 4: Impact on Block Fuel Burn.

		Oscillating Heat Pipes		Liquid / Air Heat Exchanger	
Loop	Heat Load (kW)	Block Fuel Burn, economic	Block Fuel Burn, design	Block Fuel Burn, economic*	Block Fuel Burn, design*
Battery	222	+0.10%	+0.11%	+0.19%	+0.20%
Electronics	919	+0.44%	+0.45%	+0.61%	+0.64%

    * Note: Does not include sensitivities to power required

For the SUSAN design, drag has a larger impact on block fuel burn than mass; therefore, the higher mass of the OHP still results in a lower increase to the block fuel burn than the liquid / air HEX, even without accounting for the power required for the liquid / air HEX. From an overall systems perspective, maximizing the use of OHP for TMS where practicable will be beneficial.

D. Thermal Management System for Batteries

The batteries pose a particular challenge for thermal management. The restrictive temperature limits on the batteries necessitate either highly variable thermal management or thermal isolation from the surface of the aircraft and a means of cooling that is not dependent on outside air temperature. A trade between the two options has not yet been conducted; currently the plan is to size the thermal management system using the 1% worldwide hot day cruise condition as the design case [29, 30]. The other major contributor to thermal analysis, component temperature, is allowed to vary between the upper and lower limits.

The current design places the batteries in the wings which a previous study on a similar aircraft established as a feasible location for outer mold line cooling, of which OHP is one method [31]. Since OHP result in a lower increase in block fuel burn than a liquid / air HEX, OHP seems a good option for thermal management of the batteries. Design and evaluation are underway for this part of the TMS and include determining the location of the OHP, understanding potential impacts on the design of the wing and distributed electric propulsion, and sizing the OHP. The relatively low maximum temperature limit of the batteries results in a low temperature differential with the outside air, necessitating large surface area for exchanging heat with the freestream air. Built into the wing surface itself, an OHP would not be as easy to bypass in colder weather as a traditional ram air HEX (which can just be blocked off if needed). In 1% or 20% worldwide cold day conditions, too much heat would be rejected by the OHP for the batteries to maintain temperatures within the defined limits [29]. Heaters can be used to maintain the batteries at the correct temperature. Alternatively, heat rejected from other components could be used instead using either a shared coolant loop or a liquid / liquid HEX between coolant loops. The trade between these options is still underway; calculations of the size of the OHP for each day type and excess heat rejection compared to 1% hot day conditions, summarized in Table 5, contribute to this analysis.

Table 5: OHP area and excess heat rejected per day type.

	1% Hot Day	Standard Day	20% Cold Day	1% Cold Day
OHP Area	7.2 m^2	4.1 m^2	4.2 m^2	3.9 m^2
Excess Heat Rejection	0 kW	16.26 kW	21.42 kW	25.68 kW

From the results in Table 5, a third option appears to be worth pursuing: sizing the OHP for the Standard or 20% Cold Day and providing supplemental cooling on a 1% Hot Day. It is already necessary to provide some form of supplemental cooling. These OHP sizing results are based on the cruise condition; higher temperatures and reduced air movement on the ground will necessitate additional cooling, possibly by running the cooling loop through ground support equipment to provide the necessary heat exchange. Design of the TMS for the batteries is still ongoing to address these challenging aspects of the design.

VI. Conclusions

This paper describes the current state of the development of the power and propulsion system for the SUSAN concept vehicle. The SUSAN vehicle considers a series hybrid architecture that uses a single engine to provide all propulsion needs. An engine failure would be mitigated with a battery system that can operate the propulsion system in case of emergency. It is thought that this configuration will weigh and cost less in terms of upfront cost and maintenance cost. Details of the system break down into subcomponents consisting of a turbofan engine, the electrical system, an advanced control system (TEEM), and the thermal management system. Operation points of interest covered will include sea level static, rolling takeoff, top of climb, and cruise. Here a study to optimize the thrust split ratio shows a weight advantage by making use of engine thrust over highly efficient electrically driven wing fans. Future work includes studying changes in bypass ratio and the effects on potential splitter boundary layer separation with large scale power extraction, updates in BLI for the wing propulsors and increasing the BLI fidelity of the main engine, and increasing the detail of off-design electrical system efficiency modeling. These issues are especially critical during low power or fringe cases where hardware is operating well away from expected conditions.

Updates on the electrical power system (EPS) were provided. The electric machines - the wing engine machine and the main generator – were discussed; updates were given on the requirements, topology, and approach for the EPS converters; the approach to electrical cable selection and modelling was covered; and the change in the DC bus approach from an unregulated to a regulated configuration was discussed.

For the SUSAN thermal management system, the system architecture was discussed along with future work. Propylene glycol/water was chosen as the coolant for the battery loop as a low-toxicity non-dielectric. PAO was chosen for the electrical power system loop after a survey and comparison of commercial off the shelf coolants, considering thermal performance, pumping loss, and flammability concerns. Finally, oscillating heat pipes were shown to perform better than liquid/air heat exchangers in terms of block fuel burn.

Future work on the SUSAN design effort includes engine sizing, boost sizing, and failure scenario analysis, using an integrated aircraft model.

References

[1] Jansen, Ralph, et al. "Subsonic Single Aft Engine (SUSAN) Transport Aircraft Concept and Trade Space Exploration." AIAA SciTech 2022 Forum. 2022.

[2] Mirhashemi, A., Chapman, J., Miller, C., Julia, S. and Jansen, R., 2022. Tail-mounted engine Architecture and Design for the Subsonic Single Aft Engine Electrofan Aircraft. In AIAA SCITECH 2022 Forum (p. 2182)

[3] Chapman, J. "Considering Turbofan Operability in Hybrid Electric Aircraft Propulsion System Design," To be presented at AIAA SciTech Forum, National Harbor, MD, 2023.

[4] Haglage, J.M., Dever, T.P., Jansen, R.H., Lewis, M.A., "Electrical System Trade Study for SUSAN Electrofan Concept Vehicle", AIAA SciTech Forum, AIAA 2022-2183, San Diego, CA, 2022.

[5] R. H. Jansen et al., "High Efficiency Megawatt Motor Preliminary Design," 2019 AIAA/IEEE Electric Aircraft Technologies Symposium (EATS), 2019, pp. 1-13.

[6] Jansen, R. H., De Jesus-Arce, Y. , Kascak, P. E., Dyson, R. W., Woodworth, A. A., Scheidler, J. J., Edwards, R. D., Stalcup, E. J., Wilhite, J. M., Duffy, K. D., Passe, P. J., McCormick, S. P., "High Efficiency Megawatt Motor Conceptual Design," 2018 Joint Propulsion Conference, AIAA Propulsion and Energy Forum, AIAA 2018-4699, Cincinnati, Ohio, 2018.

[7] Granger, Matthew G., et al. "Combined Analysis of NASA's High Efficiency Megawatt Motor and Its Converter." AIAA Propulsion and Energy 2021 Forum. 2021.

[8] Granger, Matthew G., et al. "Concept Design of a 1.4 MW Drive for Rotor Loss Minimization in a Partially Superconducting Motor." 2022 IEEE Transportation Electrification Conference & Expo (ITEC). IEEE, 2022.

[9] Dever, T.P., Jansen, R.H. "Cable Key Performance Parameters for Megawatt Electrified Aircraft Propulsion Conceptual Aircraft Model", IEEE/AIAA Transportation Electrification Conference and Electric Aircraft Technologies (EATS) Symposium, June, 2022.

[10] Culley, D., Kratz, J., and Thomas, G., "Turbine Electrified Energy Management (TEEM) For Enabling More Efficient Engine Designs," AIAA Propulsion & Energy Forum, Cincinnati, OH. 2018.

[11] Kratz, J., Culley, D., and Thomas, G., "A Control Strategy for Turbine Electrified Energy Management," AIAA Propulsion & Energy Forum, Indianapolis, IN. 2019.

[12] Kratz, J., and Culley, D., "Enhancement of a Conceptual Hybrid Electric Tilt-Wing Propulsion System through Application of the Turbine Electrified Energy Management Concept," AIAA 2021-0875, AIAA SciTech Forum, Virtual Conference, 2021.

[13] Kratz, J., and Simon, D., "Failure Modes and Mitigation Strategies for a Turboelectric Aircraft Concept with Turbine Electrified Energy Management," AIAA SciTech Forum, San Diego, CA. 2022.

[14] Philpot, M., "Practical Consideration In Designing the Engine Cycle," Defense Technical Information Center, 1992.

[15] Spakovszky, Z., "Instabilities Everywhere! Hard Problems in Aero-Engines," GT2021-60864, ASME Turbo Expo, June, 2021.

[16] Kratz, J., Culley, D., and Lehan, J. "Transient Optimization for the Betterment of Turbine Electrified Energy Management," AIAA SciTech 2022 Forum, National Harbor, MD. 2022.

[17] Heersema, N., and Jansen, R. Thermal Management System Trade Study for SUSAN Electrofan Aircraft. Presented at the AIAA SCITECH 2022 Forum, San Diego, CA & Virtual, 2022.

[18] Mudawar, I. "Assessment of High-Heat-Flux Thermal Management Schemes." *IEEE Transactions on Components and Packaging Technologies*, Vol. 24, No. 2, 2001, pp. 122–141. https://doi.org/10.1109/6144.926375.

[19] Zhang, Z., Wang, X., and Yan, Y. "A Review of the State-of-the-Art in Electronic Cooling." *Advances in Electrical Engineering*, 2021, p. 26.

[20] Adler, E. J., Brelje, B. J., and Martins, J. R. R. A. "Thermal Management System Optimization for a Parallel Hybrid Aircraft Considering Mission Fuel Burn." *Aerospace*, Vol. 9, No. 5, 2022, p. 243. https://doi.org/10.3390/aerospace9050243.

[21] Dyson, R. W., Rodriguez, L. A., and Roth, M. E. Solid-State Exergy Optimized Electric Aircraft Thermal and Fault Management. Presented at the AIAA Propulsion and Energy 2020 Forum, VIRTUAL EVENT, 2020.

[22] Kelly, B., Moreno, G., Myers, S., Narumanchi, S., Joshi, Y., and Graham, S. Dielectric Fluids for the Direct Forced Convection Cooling of Power Electronics. Presented at the 2021 20th IEEE Intersociety Conference on Thermal and Thermomechanical Phenomena in Electronic Systems (iTherm), San Diego, CA, USA, 2021.

[23] Gorbounov, P., Battistin, M., and Thomas, E. *Comparison of Liquid Coolants Suitable for Single-Phase Detector Cooling.* CERN, 2016.

[24] Saylor, J. R., Bar-Cohen, A., Lee Tien-Yu, Simon, T. W., Tong Wei, and Wu Pey-Shey. "Fluid Selection and Property Effects in Single- and Two-Phase Immersion Cooling (of Electronic Components)." IEEE Transactions on Components, Hybrids, and Manufacturing Technology, Vol. 11, No. 4, 1988, pp. 557–565. https://doi.org/10.1109/33.16697.

[25] Mouromtseff, I. E. "Water and Forced-Air Cooling of Vacuum Tubes Nonelectronic Problems in Electronic Tubes." Proceedings of the IRE, Vol. 30, No. 4, 1942, pp. 190–205. https://doi.org/10.1109/JRPROC.1942.234654.

[26] Heersema, N., and Jansen, R. Thermal Management System Trade Study for SUSAN Electrofan Aircraft. Presented at the AIAA SCITECH 2022 Forum, San Diego, CA & Virtual, 2022.

[27] Chau, T., Kenway, G., and Kiris, C. C. Conceptual Exploration of Aircraft Configurations for the SUSAN Electrofan. Presented at the AIAA SCITECH 2022 Forum, San Diego, CA & Virtual, 2022.

[28] Lynde, M. N., Campbell, R. L., and Hiller, B. R. A Design Exploration of Natural Laminar Flow Applications for the SUSAN Electrofan Concept. Presented at the AIAA SCITECH 2022 Forum, San Diego, CA & Virtual, 2022.

[29] SAE International. AS210: Definition of Commonly Used Day Types. SAE International, Nov, 2018.

[30] Stalcup, E. and Heersema, N. "Thermal Requirements for Design and Analysis of Subsonic Single Aft Engine (SUSAN) Research Aircraft," To be presented at AIAA SciTech Forum, National Harbor, MD, 2023.

[31] Schnulo, S. L., Chapman, J. W., Hanlon, P., Hasseeb, H., Jansen, R., Sadey, D., Sozer, E., Jensen, J., Maldonado, D., Bhamidapati, K., Heersema, N., Antcliff, K., Frederick, Z. J., and Kirk, J. Assessment of the Impact of an Advanced Power System on a Turboelectric Single-Aisle Concept Aircraft. Presented at the AIAA Propulsion and Energy 2020 Forum, VIRTUAL EVENT, 2020.